Two-Dimensional Infrared Spectroscopy of Isolated Molecular Ions

Zifan Ma, Liangyi Chen, Chuzhi Xu, and Joseph A. Fournier*

Department of Chemistry, Washington University in St. Louis, St. Louis, MO 63130

*corresponding author: jfournier@wustl.edu

Abstract

Two-dimensional infrared (2D IR) spectroscopy of mass-selected, cryogenically cooled molecular ions is presented. Nonlinear response pathways, encoded in the time-domain photodissociation action response of weakly-bound N_2 messenger tags, are isolated using pulse shaping techniques following excitation with four collinear ultrafast IR pulses. 2D IR spectra of $Re(CO)_3(CH_3CN)_3^+$ ions capture off-diagonal cross-peak bleach signals between the asymmetric and symmetric carbonyl stretching transitions which display intensity variations as a function of pump-probe delay time due to coherent coupling between the modes. Well-resolved 2D IR features in the congested fingerprint region of protonated caffeine ($C_8H_{10}N_4O_2H^+$) are also reported. Importantly, intense cross-peak signals are observed at 3 ps waiting time, indicating that tag-loss dynamics are not competing with the measured nonlinear signals. These demonstrations pave the way for more precise studies of molecular interactions and dynamics that are not easily obtainable with current condensed-phase methodologies.

1

There has been an impressive growth of experiments adapting condensed-phase ultrafast nonlinear spectroscopic methodologies for the study of molecular systems isolated in the gas phase.[1–13] Ultrafast transient and multidimensional spectroscopies provide a wealth of structural and dynamical information not easily obtained from linear spectra, such as energy transfer and relaxation dynamics, frequency correlation dynamics, orientational dynamics, and intramolecular/intermolecular interactions encoded through off-diagonal cross-peak features.[14,15] Acquisition of well-resolved nonlinear spectra of gaseous species in a controlled environment, free from solvent effects, thermal broadening, and other sources of congestion, has the potential to uncover new fundamental insights on molecular interactions and dynamics that are not currently accessible with condensed-phase methodologies. Data from such gas-phase experiments would also provide stringent benchmarks for computational predictions and aid in the interpretation of complementary condensed-phase experiments.

The merger of mass spectrometric ion processing techniques with nonlinear ultrafast spectroscopies is particularly enticing.[16–22] Soft ionization techniques such as electrospray ionization enables the extraction of complex and diverse chemical, biological, and nanomaterial systems into the gas phase from nM-µM solutions. Extracted ions can be further processed to controllably produce the desired chemical species, for example, through H-D exchange, generation of reactive intermediates, or clustering with solvent molecules.[23,24] Buffer gas cooling in cryogenic ion traps offers additional advantages by quenching molecular systems into their lowest-energy configurations. Critically, spectroscopic analyses can be performed on the precise composition-selected system of interest.

A major drawback of spectroscopic studies on gaseous ions is the low number density ($<10^6$ cm^{-3}) that can be stored in ion traps. Consequently, the direct measurement of light absorption or an emitted nonlinear signal field are not feasible. Indirect "action" responses that encode the light-matter interactions must instead be measured. In the widely used messenger tagging approach,[25] the parent ion is complexed with weakly-bound "tag" molecules (He, H_2, N_2, Ar). These complexes only form under supersonic expansion conditions or under cryogenic buffer gas cooling in an ion trap. In standard frequency-domain experiments, a high-resolution laser source (typically few to sub-cm^{-1} resolution, ns pulse duration) is frequency scanned through the optical region of interest. Resonant excitation of the parent ion results in photodissociation of the tag molecule through intramolecular vibrational redistribution (IVR) of the excitation energy[26] in the single photon regime. Measurement of the photodissociation yield as a function of laser frequency generates an action spectrum. As long as the tag binding energy is below the laser photon energy, the resulting action spectrum is directly proportional to the linear optical spectrum of the parent ion.

The application of ultrafast pulses also presents the challenge of how to frequency resolve an action response with a broadband source. Seminal work by Marcus,[27–29] Brixner,[30–32] Stienkemeier,[33–35] and others[36–39] have established the ability of indirect action responses such as fluorescence, ionization, and photofragmentation to encode nonlinear molecular responses. These responses can be frequency resolved from time-domain measurements collected using a series of pulses. Key to these experiments is the use of pulse shapers to precisely control the delays and,

crucially, phases of each pulse.[40] Phase-cycling schemes can then be applied to create and isolate the desired nonlinear signals encoded in the action response.[41]

Motivated by these studies, we have worked towards the implementation of ultrafast, frequency-resolved transient absorption (TA) and two-dimensional (2D) cryogenic ion vibrational spectroscopy (CIVS). We previously demonstrated the acquisition of linear infrared spectra of cryogenically cooled ions using an ultrafast pulse pair (Fig. 1a).[42] The tag-loss photodissociation signal oscillates as a function of the delay time, τ, between the pulses due to interferences between the excited vibrational coherences, with the Fourier transform yielding the frequency-domain linear action spectrum. Very recently, we presented the acquisition of TA-CIVS where excitation by a pump pulse precedes a probe pulse pair (Fig. 1b).[43] Data is again collected in the time domain as a function of the probe pair delay time to frequency resolve the probe axis. An eight-step phase-cycling scheme isolates the TA signal from background linear and double quantum pathways, allowing for the measurement of bleaching signals of the fundamental transitions that evolve with the pump-probe waiting time, T_w. Herein, we present the first 2D-CIVS spectra. Four collinear pulses, consisting of a pump pulse pair and a probe pulse pair, are used to excite tagged molecular ions (Fig. 1c). The tag-loss action signal is monitored as a function of both the pump pair delay, τ_1, and the probe pair delay, τ_3, using a 27-step phase-cycling scheme. A 2D-Fourier transform of the time-domain data produces a 2D IR spectrum that is frequency resolved along the
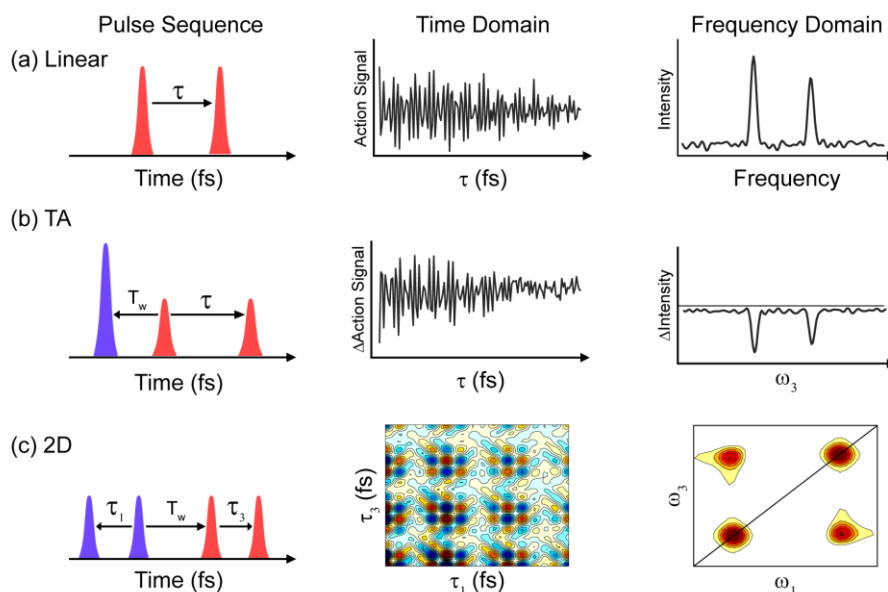
Fig. 1. Hierarchy of frequency-resolved, action-detected spectroscopies using ultrafast light pulses illustrating the respective pulse sequences, measured time-domain action signal, and processed frequency-domain spectra. (a) Linear spectra are collected by monitoring the action response as a function of the delay time τ between a pulse pair. (b) Transient absorption (TA) spectra utilize a pump pulse preceding a probe pulse pair by a waiting time T_w. The action signal is monitored as a function of the probe pair delay time τ. (c) Two-dimensional (2D) spectra are collected as a function of the delay between a pump pair (τ_1) and probe pair (τ_3). A 2D Fourier transform resolves the pump (ω_1) and probe (ω_3) frequency axes.

pump and probe axes. A detailed description of the experimental methodologies and data processing procedures are provided in Supporting Information.

We first investigate the *fac*-Re(CO)$_3$(CH$_3$CN)$_3^+$·N$_2$ complex (Fig. 2a) in the carbonyl stretch region. There are two features in the linear IR spectrum, a doubly-degenerate asymmetric carbonyl stretch near 2000 cm^{-1} and a symmetric carbonyl stretch near 2080 cm^{-1} (top panel Fig. 2b). The bottom panel of Fig. 2b presents the previously reported[43] TA-CIVS spectra at 200 fs and 400 fs waiting times, showing relatively strong bleaching signals at the two fundamental frequencies. Importantly, there are notable intensity differences between the two spectra. Our previous measurements[43] showed intensity modulations in both bleach signals with a period of ~417 fs, matching the energy difference between the two transitions. The presence of such oscillations with pump-probe waiting time are indicative of strong coherent coupling between the vibrational modes.[14,44–46] The implied presence of mode coupling are expected to manifest as off-diagonal cross peaks between the symmetric and asymmetric carbonyl stretches in a 2D IR spectrum. 2D-CIVS spectra at 208 fs (TA minimum) and 417 fs (TA maximum) waiting times are presented in Figs. 2c and 2d, respectively. Cross-peak features between the carbonyl stretch transitions are clearly recovered, as anticipated, in addition to the diagonal bleach signals. The cross peaks and overall signal are stronger at T_w = 417 fs compared to 208 fs, consistent with the TA spectra and reported solution-phase 2D IR spectra of metal-carbonyl complexes.[47,48] Note that
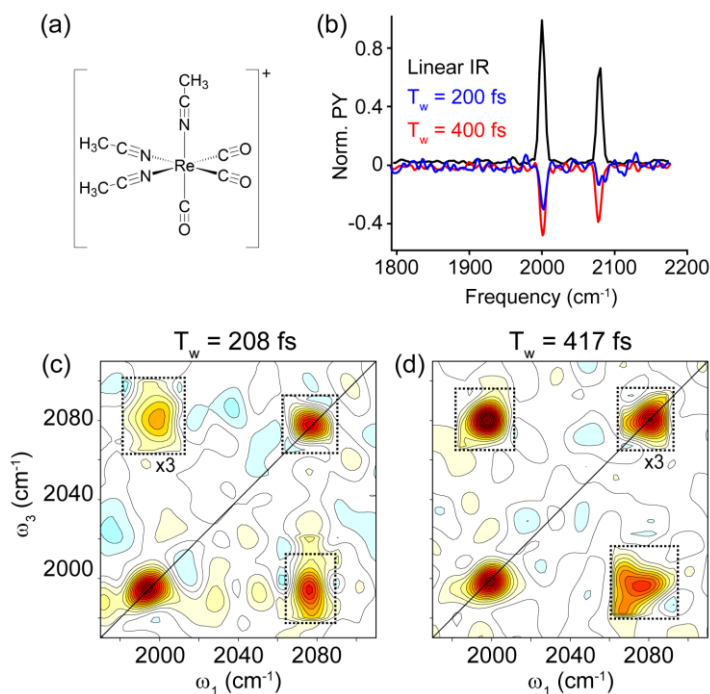
Fig. 2. (a) Structure of *fac*-Re(CO)$_3$(CH$_3$CN)$_3^+$. (b) Linear and TA-CIVS spectra at 200 fs and 400 fs waiting times in the carbonyl stretch region. (c) 2D-CIVS spectrum at 208 fs waiting time (corresponding to the TA signal minimum). (d) 2D-CIVS spectrum at 417 fs waiting time (corresponding to the TA signal maximum). Off-diagonal cross-peak features are present between the coupled asymmetric and symmetric carbonyl stretch modes. The regions outlined by dashed boxes were enhanced by 3 for better visualization.

4

the 2D-CIVS spectra were collected in the ZZZZ polarization scheme (all pulses parallel). Since the asymmetric and symmetric carbonyl stretches have orthogonal transition moments, cross-peak signal will be strongest in the ZZYY scheme. The 2D lineshapes, in general, appear homogeneously broadened with little apparent inhomogeneous diagonal elongation. This is, perhaps, not too surprising given the dilute, solvent-free environment and cryogenic conditions.
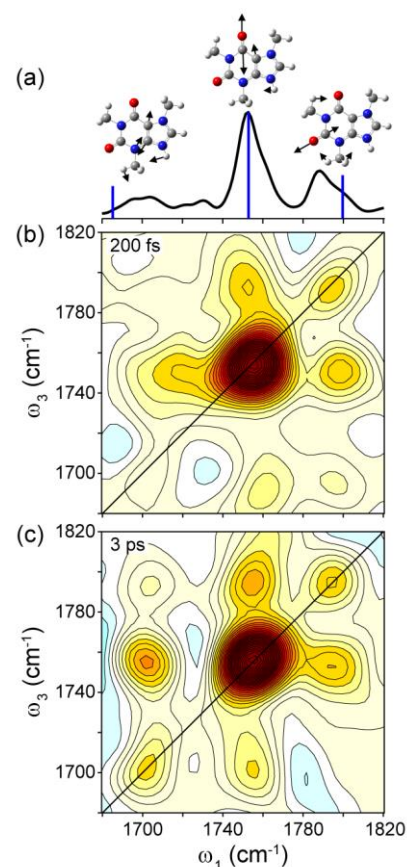
To further demonstrate that the 2D-CIVS spectra are indeed capturing nonlinear response pathways, we take a more detailed look at the asymmetric stretch bleach feature at $T_w = 417$ fs in Fig. 3. Lineshapes in 2D spectroscopies derive from both absorptive and dispersive components, leading to "phase twists" that contain positive and negative contributions.[14] In addition, nonlinear signals derive from so-called rephasing and nonrephasing pathways.[14] Rephasing (or photon echo) pathways are those where the coherences during τ_1 and τ_3 evolve in the opposite sense, with signal proportional to $e^{-i\omega_{10}(\tau_3-\tau_1)}$. Nonrephasing pathways evolve as $e^{-i\omega_{10}(\tau_3+\tau_1)}$. Feynman diagrams illustrating these pathways are provided in Supporting Information. Importantly, rephasing and nonrephasing signals produce lineshapes with opposite phase twists. Adding or simultaneously collecting the rephasing and nonrephasing signals produces purely absorptive lineshapes. The 27-step phase-cycling scheme allows the absorptive, rephasing, and nonrephasing signals to be isolated from the same data set,[41,49] the real components of which are presented in Figs. 3a, 3b, and 3c, respectively, for the asymmetric carbonyl stretch. The respective imaginary components are presented in Supporting Information. The rephasing and nonrephasing spectra for both the real and imaginary components display the appropriate phase twists[14,49,50] due to positive (blue) and negative (red) contributions to the lineshapes. These comparisons unequivocally show that the measured tag-loss photodissociation signal encodes the desired nonlinear light-matter interaction pathways.
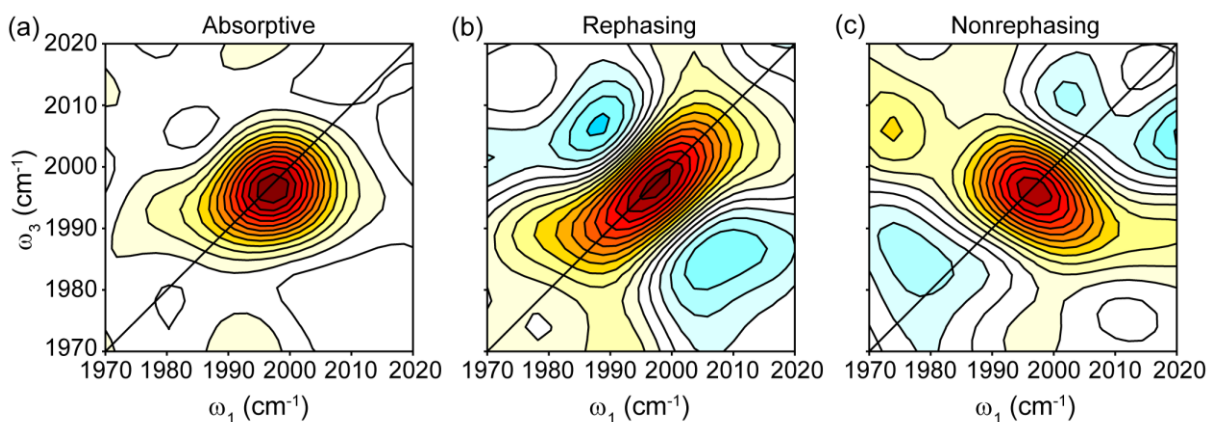
Fig. 3. (a) Absorptive, (b) rephasing, and (c) nonrephasing signals of the asymmetric carbonyl stretch in *fac*-Re(CO)$_3$(CH$_3$CN)$_3$$^+$ shown in Fig. 2d isolated through phase cycling. The rephasing and nonrephasing signals illustrate the expected phase twists due to contributions from absorptive and dispersive lineshape components.

Conspicuously absent from the absorptive 2D-CIVS spectra are positive induced absorption peaks deriving from overtone (diagonal) and combination band (off-diagonal) transitions that are hallmarks of condensed-phase experiments. The absence of induced absorption transitions is a consequence of the action-detection scheme. The action-response signal is directly proportional to the final excited-state population that causes the action. The requirement that the final state of the system be a population state necessitates the use of an additional probe pulse in action schemes. In condensed-phase experiments, the system returns to a population state after emitting a signal field, which is directly detected, following excitation by a single probe pulse. Therefore, while conventional condensed-phase approaches are 3rd-order experiments, action-based methods are actually 4th-order experiments.

This important difference results in a unique set of light-matter interaction pathways in action-detection experiments,[1,30,51] the Feynman diagrams for which are given in Supporting Information. While action experiments result in pathways analogous to the 3rd-order ground-state bleach, stimulated emission, and induced absorption pathways, there is an additional excited-state pathway not accessible in 3rd-order experiments. This new pathway, which corresponds to a bleach of the excited state, destructively interferes with the induced absorption pathway. As a result, only bleaching signals are expected in action-based TA and 2D spectra.[27,30]

Although important molecular and dynamical information provided by induced absorption transitions are unavailable, the presence of bleach-induced absorption peak pairs in condensed-phase measurements often leads to significant spectral congestion in 2D IR spectra. This is particularly true for large molecules, like peptides, in the important fingerprint region. The lack of induced absorption features, along with the much sharper spectral transitions generally obtained with CIVS, could greatly aid in the interpretation of 2D spectra. As an example, the 2D-CIVS spectrum of protonated caffeine ($C_8H_{10}N_4O_2H^+$) in the 1650-1850 cm^{-1} region is presented in Fig. 4. The linear spectrum is given in Fig. 4a along with the calculated stick spectrum.[52] There are three closely spaced transitions: the stretching modes of the two carbonyl groups and a mixed NH[+] bending/CN stretching mode. Note that the two carbonyl stretches in neutral caffeine produce an asymmetric/symmetric stretch normal mode pair that results in strong 2D IR cross peak signals in solution.[53] The calculated displacement vectors shown in Fig. 4a, however, indicate that protonation acts

Fig. 4. (a) Linear IR spectrum of protonated caffeine with calculated (B3LYP/6-311G(d,p), scaled by 0.99) stick spectrum and displacement vectors in the carbonyl stretch region. (b) 2D-CIVS spectrum at 200 fs waiting time. (c) 2D-CIVS spectrum at 3 ps waiting time. The 2D spectra display distinct cross peaks between the three main transitions. The spectrum at 3 ps shows slightly stronger cross-peak signatures.

6

to largely decouple the carbonyl stretch transitions. The NH$^+$ bend/CN stretch normal mode also appears mostly isolated from the carbonyl stretches. Despite the expectation of weaker coupling compared to neutral caffeine, the 2D-CIVS spectrum of protonated caffeine reveals relatively strong cross-peak signals between all three transitions at both 200 fs (Fig. 4b) and 3 ps (Fig. 4c) waiting times. This observation indicates the presence of anharmonic coupling between the three transitions, not unlike the coupling observed in condensed-phase 2D IR between amide I (CO stretch) and amide II (NH bend/CN stretch) modes in peptides.[54–56] Importantly, all 2D bleach features are well resolved and free from significant spectral overlap and lineshape distortions.

A critical question regarding TA and 2D-CIVS is whether tag-loss dynamics interfere in the measurement of the desired nonlinear signals of the underlying parent ion. The strong cross peaks observed at 3 ps waiting time in Fig. 4c indicate that tag-loss dynamics are not yet affecting the measurements. If tag loss occurs during the pump-probe waiting time period, the experiment becomes analogous to hole-burning: the pump acts to deplete tagged ion population causing less action signal to be produced by the probe. This would then result in static bleach signals along the diagonal and, importantly, no cross peak signals. It is evident that this is not the case for protonated caffeine. Instead, both intramolecular and intermolecular vibrational relaxation processes appear to occur on relatively long timescales. Solution-phase studies on neutral caffeine measured ~800 fs IVR timescales for the carbonyl stretches with a small solvent dependence.[53] While it is difficult to make quantitative conclusions at the current level of experimental uncertainty, the cross peaks qualitatively appear stronger and more distinct at 3 ps compared to 200 fs, suggesting vibrational energy transfer dynamics between the three modes. Intermolecular relaxation to solvent in neutral caffeine, on the other hand, was measured to occur on ~5 ps (D$_2$O) and ~10 ps (CH$_3$CN) timescales, respectively.[53] Intermolecular relaxation in isolated, cryogenically cooled protonated caffeine to a weakly interacting N$_2$ tag molecule, therefore, likely takes place on timescales >>10 ps. Similarly, the oscillatory intensity modulations measured in our previous TA-CIVS experiments on *fac*-Re(CO)$_3$(CH$_3$CN)$_3$$^+$ persisted beyond 3 ps waiting time.[43] While not completely general, we posit that intermolecular vibrational relaxation to weakly-bound tags and subsequent tag-loss dynamics will, in most cases, take place on timescales much longer than the dynamics of interest for cryogenically cooled molecular ions.

With these successful demonstrations, we envision 2D-CIVS to be a powerful tool for structure determination and the study of intramolecular and intermolecular interactions through the recovery of well-resolved off-diagonal cross peaks. For example, the amide I and amide II spectral regions in peptides are highly congested and difficult to resolve at the amino acid level with condensed-phase 2D IR without the use of isotopic labeling.[57–59] While traditional CIVS affords higher frequency resolution (linewidths typically 5-10 cm^{-1}), experiments on small peptide systems usually require comparisons to computational predictions of many conformers and/or double resonance experiments to make structural identifications.[60–65] Well-resolved cross peaks across the amide I and II regions with 2D-CIVS will help guide conformational searches and provide less ambiguity in structural assignments. Another intriguing example would be the study of biomolecule-water interactions. Solvation shell interactions are incredibly difficult to study with condensed-phase 2D IR due to the overwhelming background water signal and bulk water's rapid vibrational dynamics.[66,67] Well-established clustering techniques[68–73] can be used to study

7

biomolecule-water interactions one water molecule at a time. Ultrafast pulses provide sufficient bandwidth to interrogate the amide I, amide II, and water bend transitions simultaneously. Therefore, biomolecule-water cross peaks will directly report on the water binding sites. Alternatively, if sub-ps dynamics are not critical, pulse shaping can also be used to collect spectra more rapidly in the frequency domain using few cm^{-1} (few ps) bandwidth pump and/or probe pulses.

Ultrafast time resolution would be required for the study of strongly H-bonded systems, where H-bonded OH or NH groups often display surprisingly broad transitions even under cryogenic conditions.[74–77] This spectral breadth is predicted to arise from strong anharmonic coupling to lower-frequency modes, which will result in rapid relaxation dynamics of the excited OH/NH stretch.[78–83] TA and 2D-CIVS can be used to track the vibrational energy relaxation pathways in these systems. Further, 2D-CIVS would be able to reveal homogeneous vs. inhomogeneous contributions to broad OH/NH stretch lineshapes and track frequency-frequency correlation dynamics (spectral diffusion) as energy relaxes into low-frequency soft modes. Finally, vibrational dynamics on excited electronic states can be measured using UV/Vis pump-IR probe TA-CIVS, providing an exciting possible avenue for the study of photoinduced reaction dynamics and mechanisms.

Supporting Information (appended below)

Experimental methods and data processing procedures; Imaginary rephasing, nonrephasing, and absorptive lineshapes; Feynman diagrams for 4th-order rephasing and nonrephasing pathways for uncoupled and coupled two-oscillator systems.

Acknowledgments

Notes

The authors declare no competing financial interest.

References

(1)   Grimberg, B. I.; Lozovoy, V. V.; Dantus, M.; Mukamel, S. Ultrafast Nonlinear Spectroscopic Techniques in the Gas Phase and Their Density Matrix Representation. *J. Phys. Chem. A* **2002**, *106* (5), 697–718.

(2)   Mandal, A.; Pack, G. N.; Shah, P. P.; Erramilli, S.; Ziegler, L. D. Ultrafast Two-Dimensional Infrared Spectroscopy of a Quasifree Rotor: J Scrambling and Perfectly Anticorrelated Cross Peaks. *Phys. Rev. Lett.* **2018**, *120* (10), 6.

(3)   Silfies, M. C.; Kowzan, G.; Lewisa, N.; Allison, T. K. Broadband Cavity-Enhanced Ultrafast Spectroscopy. *Phys. Chem. Chem. Phys.* **2021**, *23*, 9743–9752.

(4)   Daniels, D. A.; Wells, T. A.; Chen, P. C. High Resolution Two-Dimensional Infrared (HR-2DIR) Spectroscopy of Gas Phase Molecules. *J. Chem. Phys.* **2022**, *157* (18), 184201.

(5)   Shipman, S. T.; Douglass, P. C.; Yoo, H. S.; Hinkle, C. E.; Mierzejewski, E. L.; Pate, B. H. Vibrational Dynamics of Carboxylic Acid Dimers in Gas and Dilute Solution. *Phys. Chem. Chem. Phys.* **2007**, *9* (32), 4572–4586.

(6)   Schriever, C.; Lochbrunner, S.; Riedle, E.; Nesbitt, D. J. Ultrasensitive Ultraviolet-Visible 20 fs Absorption Spectroscopy of Low Vapor Pressure Molecules in the Gas Phase. *Rev. Sci. Instrum.* **2008**, *79* (1), 013107.

(7)   Cole-Filipiak, N. C.; Troß, J.; Schrader, P.; McCaslin, L. M.; Ramasesha, K. Ultraviolet Photodissociation of Gas-Phase Iron Pentacarbonyl Probed with Ultrafast Infrared Spectroscopy. *J. Chem. Phys.* **2021**, *154* (13), 134308.

(8)   Cole-Filipiak, N. C.; Troß, J.; Schrader, P.; McCaslin, L. M.; Ramasesha, K. Ultrafast Infrared Transient Absorption Spectroscopy of Gas-Phase $Ni(CO)_4$ Photodissociation at 261 nm. *J. Chem. Phys.* **2022**, *156* (14), 144306.

(9)   Schnorr, K.; Belina, M.; Augustin, S.; Lindenblatt, H.; Liu, Y.; Meister, S.; Pfeifer, T.; Schmid, G.; Treusch, R.; Trost, F.; Slavíček, P.; Moshammer, R. Direct Tracking of Ultrafast Proton Transfer in Water Dimers. *Sci. Adv.* **2023**, *9* (28), eadg7864.

(10) Heald, L. F.; Gosman, R. S.; Rotteger, C. H.; Jarman, C. K.; Sayres, S. G. Nonadiabatic Photodissociation and Dehydrogenation Dynamics of N-Butyl Bromide Following p-Rydberg Excitation. *J. Phys. Chem. Lett.* **2023**, *14* (27), 6278–6285.

(11) Wolf, T. J. A.; Parrish, R. M.; Myhre, R. H.; Martínez, T. J.; Koch, H.; Gühr, M. Observation of Ultrafast Intersystem Crossing in Thymine by Extreme Ultraviolet Time-Resolved Photoelectron Spectroscopy. *J. Phys. Chem. A* **2019**, *123* (32), 6897–6903.

(12) Zettergren, H.; Domaracka, A.; Schlathölter, T.; Bolognesi, P.; Díaz-Tendero, S.; Łabuda, M.; Tosic, S.; Maclot, S.; Johnsson, P.; Steber, A.; Tikhonov, D; *et al.* A. Roadmap on Dynamics of Molecules and Clusters in the Gas Phase. *Eur. Phys. J. D* **2021**, *75* (5), 152.

(13) Wang, E.; Kling, N. G.; LaForge, A. C.; Obaid, R.; Pathak, S.; Bhattacharyya, S.; Meister, S.; Trost, F.; Lindenblatt, H.; Schoch, P.; *et al.* Ultrafast Roaming Mechanisms in Ethanol Probed by Intense Extreme Ultraviolet Free-Electron Laser Radiation: Electron Transfer versus Proton Transfer. *J. Phys. Chem. Lett.* **2023**, *14* (18), 4372–4380.

(14) Hamm, P.; Zanni, M. *Concepts and Methods of 2D Infrared Spectroscopy*; Cambridge University Press, 2011.

(15) Cho, M. Coherent Two-Dimensional Optical Spectroscopy. *Chem. Rev.* **2008**, *108* (4), 1331–1418.

(16) Veenstra, A. P.; Monzel, L.; Baksi, A.; Czekner, J.; Lebedkin, S.; Schneider, E. K.; Pradeep, T.; Unterreiner, A.-N.; Kappes, M. M. Ultrafast Intersystem Crossing in Isolated $Ag_{29}(BDT)_{123}{}^-$ Probed by Time-Resolved Pump–Probe Photoelectron Spectroscopy. *J. Phys. Chem. Lett.* **2020**, *11* (7), 2675–2681.

9

(17) Bull, J. N.; West, C. W.; Anstöter, C. S.; Silva, G. da; Bieske, E. J.; Verlet, J. R. R. Ultrafast Photoisomerisation of an Isolated Retinoid. *Phys. Chem. Chem. Phys.* **2019**, *21* (20), 10567–10579.

(18) Schüssler, L.; Israil, R. G. E.; Hütchen, P.; Thiel, W. R.; Diller, R.; Riehn, C. Ultrafast Spectroscopy of RuII Polypyridine Complexes in the Gas Phase and the Liquid Phase: $[Ru(2,2'-Bipyridine)_2(Nicotinamide)_2]^{2+}$. *Phys. Chem. Chem. Phys.* **2023**, *25* (6), 4899–4914.

(19) Gruber, E.; Kabylda, A. M.; Nielsen, M. B.; Rasmussen, A. P.; Teiwes, R.; Kusochek, P. A.; Bochenkova, A. V.; Andersen, L. H. Light Driven Ultrafast Bioinspired Molecular Motors: Steering and Accelerating Photoisomerization Dynamics of Retinal. *J. Am. Chem. Soc.* **2022**, *144* (1), 69–73.

(20) Guyon, L.; Tabarin, T.; Thuillier, B.; Antoine, R.; Broyer, M.; Boutou, V.; Wolf, J. P.; Dugourd, P. Femtosecond Pump-Probe Experiments on Trapped Flavin: Optical Control of Dissociation. *J. Chem. Phys.* **2008**, *128* (7), 5.

(21) MacAleese, L.; Hermelin, S.; El Hage, K.; Chouzenoux, P.; Kulesza, A.; Antoine, R.; Bonacina, L.; Meuwly, M.; Wolf, J. P.; Dugourd, P. Sequential Proton Coupled Electron Transfer (PCET): Dynamics Observed Over 8 Orders of Magnitude in Time. *J. Am. Chem. Soc.* **2016**, *138* (13), 4401–4407.

(22) Marlton, S. J. P.; McKinnon, B. I.; Greißel, P.; Shiels, O. J.; Ucur, B.; Trevitt, A. J. Picosecond Excited-State Lifetimes of Protonated Indazole and Benzimidazole: The Role of the N–N Bond. *J. Chem. Phys.* **2021**, *155* (18), 184302.

(23) Wolk, A. B.; Leavitt, C. M.; Garand, E.; Johnson, M. A. Cryogenic Ion Chemistry and Spectroscopy. *Acc. Chem. Res.* **2014**, *47* (1), 202–210.

(24) Garand, E. Spectroscopy of Reactive Complexes and Solvated Clusters: A Bottom-Up Approach Using Cryogenic Ion Traps. *J. Phys. Chem. A* **2018**, *122* (32), 6479–6490.

(25) Okumura, M.; Yeh, L. I.; Myers, J. D.; Lee, Y. T. Infrared Spectra of the Cluster Ions $H_7O_3^+\cdot H_2$ and $H_9O_4^+\cdot H_2$. *J. Chem. Phys.* **1986**, *85* (4), 2328–2329.

(26) Nesbitt, D. J.; Field, R. W. Vibrational Energy Flow in Highly Excited Molecules: Role of Intramolecular Vibrational Redistribution. *J. Phys. Chem.* **1996**, *100* (31), 12735–12756.

(27) Tekavec, P. F.; Lott, G. A.; Marcus, A. H. Fluorescence-Detected Two-Dimensional Electronic Coherence Spectroscopy by Acousto-Optic Phase Modulation. *J. Chem. Phys.* **2007**, *127* (21), 214307.

(28) Tekavec, P. F.; Dyke, T. R.; Marcus, A. H. Wave Packet Interferometry and Quantum State Reconstruction by Acousto-Optic Phase Modulation. *J. Chem. Phys.* **2006**, *125* (19), 19.

(29) Sanders, J. N.; Saikin, S. K.; Mostame, S.; Andrade, X.; Widom, J. R.; Marcus, A. H.; Aspuru-Guzik, A. Compressed Sensing for Multidimensional Spectroscopy Experiments. *J. Phys. Chem. Lett.* **2012**, *3* (18), 2697–2702.

(30) Maly, P.; Brixner, T. Fluorescence-Detected Pump-Probe Spectroscopy. *Angew. Chem. Int. Ed.* **2021**, *60* (34), 18867–18875.

(31) Roeding, S.; Brixner, T. Coherent Two-Dimensional Electronic Mass Spectrometry. *Nat. Commun.* **2018**, *9* (1), 2519.

(32) Lüttig, J.; Mueller, S.; Malý, P.; Krich, J. J.; Brixner, T. Higher-Order Multidimensional and Pump–Probe Spectroscopies. *J. Phys. Chem. Lett.* **2023**, *14* (33), 7556–7573.

10

(33)   Bruder, L.; Bangert, U.; Binz, M.; Uhl, D.; Vexiau, R.; Bouloufa-Maafa, N.; Dulieu, O.; Stienkemeier, F. Coherent Multidimensional Spectroscopy of Dilute Gas-Phase Nanosystems. *Nat. Commun.* **2018**, *9* (1), 4823.

(34)   Bruder, L.; Bangert, U.; Binz, M.; Uhl, D.; Stienkemeier, F. Coherent Multidimensional Spectroscopy in the Gas Phase. *J. Phys. B- Mol. Opt. Phys.* **2019**, *52* (18), 183501.

(35)   Mudrich, M.; Heister, Ph.; Hippler, T.; Giese, Ch.; Dulieu, O.; Stienkemeier, F. Spectroscopy of Triplet States of Rb_2 by Femtosecond Pump-Probe Photoionization of Doped Helium Nanodroplets. *Phys. Rev. A* **2009**, *80* (4), 042512.

(36)   Scherer, N. F.; Carlson, R. J.; Matro, A.; Du, M.; Ruggiero, A. J.; Romerorochin, V.; Cina, J. A.; Fleming, G. R.; Rice, S. A. Fluorescence-Detected Wave Packet Interferometry - Time Resolved Molecular-Spectroscopy with Sequences of Femtosecond Phase-Locked Pulses. *J. Chem. Phys.* **1991**, *95* (3), 1487–1511.

(37)   Nikaido, M.; Mizuse, K.; Ohshima, Y. Torsional Wave-Packet Dynamics in 2-Fluorobiphenyl Investigated by State-Selective Ionization-Detected Impulsive Stimulated Raman Spectroscopy. *J. Phys. Chem. A* **2023**, *127* (23), 4964–4978.

(38)   Nardin, G.; Autry, T. M.; Silverman, K. L.; Cundiff, S. T. Multidimensional Coherent Photocurrent Spectroscopy of a Semiconductor Nanostructure. *Opt. Express* **2013**, *21* (23), 28617–28627.

(39)   Liebel, M.; Toninelli, C.; van Hulst, N. F. Room-Temperature Ultrafast Nonlinear Spectroscopy of a Single Molecule. *Nat. Photonics* **2018**, *12* (1), 45–49.

(40)   Shim, S.-H.; Strasfeld, D. B.; Ling, Y. L.; Zanni, M. T. Automated 2D IR Spectroscopy Using a Mid-IR Pulse Shaper and Application of This Technology to the Human Islet Amyloid Polypeptide. *Proc. Natl. Acad. Sci.* **2007**, *104* (36), 14197–14202.

(41)   Yan, S.; Tan, H.-S. Phase Cycling Schemes for Two-Dimensional Optical Spectroscopy with a Pump–Probe Beam Geometry. *Chem. Phys.* **2009**, *360* (1), 110–115.

(42)   Chen, L.; Dean, J. L. S.; Fournier, J. A. Time-Domain Vibrational Action Spectroscopy of Cryogenically Cooled, Messenger-Tagged Ions Using Ultrafast IR Pulses. *J. Phys. Chem. A* **2021**, *125* (47), 10235–10244.

(43)   Chen, L.; Ma, Z.; Fournier, J. A. Ultrafast Transient Vibrational Action Spectroscopy of Cryogenically Cooled Ions. *J. Chem. Phys.* **2023**, *159* (4), 041101.

(44)   Golonzka, O.; Tokmakoff, A. Polarization-Selective Third-Order Spectroscopy of Coupled Vibronic States. *J. Chem. Phys.* **2001**, *115*, 297.

(45)   King, J. T.; Baiz, C. R.; Kubarych, K. J. Solvent-Dependent Spectral Diffusion in a Hydrogen Bonded "Vibrational Aggregate." *J. Phys. Chem. A* **2010**, *114* (39), 10590–10604.

(46)   Kiefer, L. M.; King, J. T.; Kubarych, K. J. Equilibrium Excited State Dynamics of a Photoactivated Catalyst Measured with Ultrafast Transient 2DIR. *J. Phys. Chem. A* **2014**, *118* (42), 9853–9860.

(47)   Baiz, C. R.; McRobbie, P. L.; Anna, J. M.; Geva, E.; Kubarych, K. J. Two-Dimensional Infrared Spectroscopy of Metal Carbonyls. *Acc. Chem. Res.* **2009**, *42* (9), 1395–1404.

(48)   Khalil, M.; Demirdoven, N.; Tokmakoff, A. Coherent 2D IR Spectroscopy: Molecular Structure and Dynamics in Solution. *J. Phys. Chem. A* **2003**, *107* (27), 5258–5279.

(49)   De, A. K.; Monahan, D.; Dawlaty, J. M.; Fleming, G. R. Two-Dimensional Fluorescence-Detected Coherent Spectroscopy with Absolute Phasing by Confocal Imaging of a Dynamic Grating and 27-Step Phase-Cycling. *J. Chem. Phys.* **2014**, *140* (19), 194201.

(50) Mueller, S.; Brixner, T. Molecular Coherent Three-Quantum Two-Dimensional Fluorescence Spectroscopy. *J. Phys. Chem. Lett.* **2020**, *11* (13), 5139–5147.

(51) Mukamel, S. *Principles of Nonlinear Optical Spectroscopy*; Principles of Nonlinear Optical Spectroscopy; Oxford University Press: New York, 1995.

(52) Frisch, M. J.; Trucks, G. W.; Schlegel, H. B.; Scuseria, G. E.; Robb, M. A.; Cheeseman, J. R.; Scalmani, G.; Barone, V.; Mennucci, B.; Petersson, G. A.; Nakatsuji, H.; Caricato, M.; Fox, D. J.; *et al. Gaussian 09*; Gaussian, Inc.: Wallingford, CT, USA, 2009.

(53) Hanes, A. T.; Grieco, C.; Lalisse, R. F.; Hadad, C. M.; Kohler, B. Vibrational Relaxation by Methylated Xanthines in Solution: Insights from 2D IR Spectroscopy and Calculations. *J. Chem. Phys.* **2023**, *158* (4), 044302.

(54) DeFlores, L. P.; Ganim, Z.; Nicodemus, R. A.; Tokmakoff, A. Amide I′–II′ 2D IR Spectroscopy Provides Enhanced Protein Secondary Structural Sensitivity. *J. Am. Chem. Soc.* **2009**, *131* (9), 3385–3391.

(55) Maekawa, H.; Ballano, G.; Toniolo, C.; Ge, N.-H. Linear and Two-Dimensional Infrared Spectroscopic Study of the Amide I and II Modes in Fully Extended Peptide Chains. *J. Phys. Chem. B* **2011**, *115* (18), 5168–5182.

(56) Bloem, R.; Dijkstra, A. G.; Jansen, T. la C.; Knoester, J. Simulation of Vibrational Energy Transfer in Two-Dimensional Infrared Spectroscopy of Amide I and Amide II Modes in Solution. *J. Chem. Phys.* **2008**, *129* (5), 055101.

(57) Roy, S.; C. Jansen, T. L.; Knoester, J. Structural Classification of the Amide I Sites of a β-Hairpin with Isotope Label 2DIR Spectroscopy. *Phys. Chem. Chem. Phys.* **2010**, *12* (32), 9347–9357.

(58) Backus, E. H. G.; Bloem, R.; Donaldson, P. M.; Ihalainen, J. A.; Pfister, R.; Paoli, B.; Caflisch, A.; Hamm, P. 2D-IR Study of a Photoswitchable Isotope-Labeled α-Helix. *J. Phys. Chem. B* **2010**, *114* (10), 3735–3740.

(59) Kratochvil, H. T.; Carr, J. K.; Matulef, K.; Annen, A. W.; Li, H.; Maj, M.; Ostmeyer, J.; Serrano, A. L.; Raghuraman, H.; Moran, S. D.; Skinner, J. L.; Perozo, E.; Roux, B.; Valiyaveetil, F. I.; Zanni, M. T. Instantaneous Ion Configurations in the K^+ Ion Channel Selectivity Filter Revealed by 2D IR Spectroscopy. *Science* **2016**, *353* (6303), 1040–1044. DOI:

(60) Kwon, J. H.; Lee, M. J.; Song, G.; Tsuruta, K.; Ishiuchi, S.; Fujii, M.; Kang, H. Cryogenic Ion Spectroscopy of a Singly Protonated Peptide DYYVVR: Locating Phosphorylation Sites of a Kinase Domain. *J. Phys. Chem. Lett.* **2020**, *11* (17), 7103–7108.

(61) Rizzo, T. R.; Boyarkin, O. V. *Cryogenic Methods for the Spectroscopy of Large, Biomolecular Ions. in Gas-Phase IR Spectroscopy and Structure of Biological Molecules*; Rijs, A. M., Oomens, J., Eds.; Topics in Current Chemistry; Springer International Publishing: Cham, 2015; pp 43–97.

(62) Burke, N. L.; DeBlase, A. F.; Redwine, J. G.; Hopkins, J. R.; McLuckey, S. A.; Zwier, T. S. Gas-Phase Folding of a Prototypical Protonated Pentapeptide: Spectroscopic Evidence for Formation of a Charge-Stabilized β-Hairpin. *J. Am. Chem. Soc.* **2016**, *138* (8), 2849–2857.

(63) Dunbar, R. C.; Steill, J. D.; Polfer, N. C.; Oomens, J. Gas-Phase Infrared Spectroscopy of the Protonated Dipeptides H^+PheAla and H^+AlaPhe Compared to Condensed-Phase Results. *Int. J. Mass Spectrom.* **2009**, *283* (1), 77–84.

(64)   Gorbachev, V.; Tsybizova, A.; Miloglyadova, L.; Chen, P. Increasing Complexity in a Conformer Space Step-by-Step: Weighing London Dispersion against Cation - π Interactions. *J. Am. Chem. Soc.* **2022**, *144* (20), 9007–9022.

(65)   Voss, J. M.; Fischer, K. C.; Garand, E. Revealing the Structure of Isolated Peptides: IR-IR Predissociation Spectroscopy of Protonated Triglycine Isomers. *J. Mol. Spectrosc.* **2018**, *347*, 28–34.

(66)   Rutherford, S. H.; Greetham, G. M.; Parker, A. W.; Nordon, A.; Baker, M. J.; Hunt, N. T. Measuring Proteins in H_2O Using 2D-IR Spectroscopy: Pre-Processing Steps and Applications toward a Protein Library. *J. Chem. Phys.* **2022**, *157* (20), 205102.

(67)   Drozdov, A. N.; Grossfield, A.; Pappu, R. V. Role of Solvent in Determining Conformational Preferences of Alanine Dipeptide in Water. *J. Am. Chem. Soc.* **2004**, *126* (8), 2574–2581.

(68)   Saparbaev, E.; Aladinskaia, V.; Zviagin, A.; Boyarkin, O. V. Microhydration of Biomolecules: Revealing the Native Structures by Cold Ion IR Spectroscopy. *J. Phys. Chem. Lett.* **2021**, *12* (2), 907–911.

(69)   Marsh, B. M.; Voss, J. M.; Garand, E. A Dual Cryogenic Ion Trap Spectrometer for the Formation and Characterization of Solvated Ionic Clusters. *J. Chem. Phys.* **2015**, *143* (20), 204201.

(70)   Racow, E. E.; Kreinbihl, J. J.; Cosby, A. G.; Yang, Y.; Pandey, A.; Boros, E.; Johnson, C. J. General Approach to Direct Measurement of the Hydration State of Coordination Complexes in the Gas Phase: Variable Temperature Mass Spectrometry. *J. Am. Chem. Soc.* **2019**, *141* (37), 14650–14660.

(71)   Wyttenbach, T.; Bowers, M. T. Hydration of Biomolecules. *Chem. Phys. Lett.* **2009**, *480* (1), 1–16.

(72)   Heiles, S.; Cooper, R. J.; DiTucci, M. J.; Williams, E. R. Hydration of Guanidinium Depends on Its Local Environment. *Chem. Sci.* **2015**, *6* (6), 3420–3429.

(73)   Nagornova, N. S.; Rizzo, T. R.; Boyarkin, O. V. Interplay of Intra- and Intermolecular H-Bonding in a Progressively Solvated Macrocyclic Peptide. *Science* **2012**, *336* (6079), 320–323.

(74)   Chen, L.; Ma, Z.; Fournier, J. A. Origins of the Diffuse Shared Proton Vibrational Signatures in Proton-Coupled Electron Transfer Model Dyad Complexes. *J. Chem. Phys.* **2022**, *157* (15), 11.

(75)   Craig, S. M.; Menges, F. S.; Duong, C. H.; Denton, J. K.; Madison, L. R.; McCoy, A. B.; Johnson, M. A. Hidden Role of Intermolecular Proton Transfer in the Anomalously Diffuse Vibrational Spectrum of a Trapped Hydronium Ion. *Proc. Natl. Acad. Sci.* **2017**, *114* (24), E4706–E4713.

(76)   Wolke, C. T.; DeBlase, A. F.; Leavitt, C. M.; McCoy, A. B.; Johnson, M. A. Diffuse Vibrational Signature of a Single Proton Embedded in the Oxalate Scaffold, $HO_2CCO_2^-$. *J. Phys. Chem. A* **2015**, *119* (52), 13018–13024.

(77)   Johnson, C. J.; Dzugan, L. C.; Wolk, A. B.; Leavitt, C. M.; Fournier, J. A.; McCoy, A. B.; Johnson, M. A. Microhydration of Contact Ion Pairs in $M^{2+}OH^-(H_2O)_{n=1-5}$ (M = Mg, Ca) Clusters: Spectral Manifestations of a Mobile Proton Defect in the First Hydration Shell. *J. Phys. Chem. A* **2014**, *118* (35), 7590–7597.

(78)   Hamm, P.; Stock, G. Nonadiabatic Vibrational Dynamics in the $HCO_2^-·H_2O$ Complex. *J. Chem. Phys.* **2015**, *143* (13), 12.

(79) Florio, G. M.; Zwier, T. S.; Myshakin, E. M.; Jordan, K. D.; Sibert, E. L. Theoretical Modeling of the OH Stretch Infrared Spectrum of Carboxylic Acid Dimers Based on First-Principles Anharmonic Couplings. *J. Chem. Phys.* **2003**, *118* (4), 1735–1746.

(80) Yang, N.; Duong, C. H.; Kelleher, P. J.; Johnson, M. A. Capturing Intrinsic Site-Dependent Spectral Signatures and Lifetimes of Isolated OH Oscillators in Extended Water Networks. *Nat. Chem.* **2020**, *12* (2), 159–164.

(81) Zabuga, A. V.; Kamrath, M. Z.; Rizzo, T. R. Franck–Condon-like Progressions in Infrared Spectra of Biological Molecules. *J. Phys. Chem. A* **2015**, *119* (42), 10494–10501.

(82) Sibert, E. L. I.; Blodgett, K. N.; Zwier, T. S. Spectroscopic Manifestations of Indirect Vibrational State Mixing: Novel Anharmonic Effects on a Prereactive H Atom Transfer Surface. *J. Phys. Chem. A* **2021**, *125* (33), 7318–7330.

(83) Heine, N.; Kratz, E. G.; Bergmann, R.; Schofield, D. P.; Asmis, K. R.; Jordan, K. D.; McCoy, A. B. Vibrational Spectroscopy of the Water–Nitrate Complex in the O–H Stretching Region. *J. Phys. Chem. A* **2014**, *118* (37), 8188–8197.

Supporting Information for:

Two-Dimensional Infrared Spectroscopy of Isolated Molecular Ions

Zifan Ma, Liangyi Chen, Chuzhi Xu, and Joseph A. Fournier*

Department of Chemistry, Washington University in St. Louis, St. Louis, MO 63130

*corresponding author: jfournier@wustl.edu

Table of Contents:

I. Ion generation

The WUSTL cryogenic ion photofragmentation mass spectrometer has been described in more detail elsewhere.[1] Briefly, 700 µmol/L solutions of $Re(CO)_5Cl$ or caffeine were prepared in acetonitrile. Trace amount of formic acid was added to the caffeine solution to protonate it. The solution was ionized with an electrospray ion source (ESI) and guided through three differentially pumped chambers with RF-only hexapole ion guides into a three-dimensional Paul trap (Jordan TOF) attached to a closed-cycle helium cryostat (Janis Research). Helium buffer gas was introduced into the ion trap through a pulse valve (Parker Hannifin, Series 9 general valve) and the ions were collisionally cooled to 28 K. Formation of "tagged" complexes between parent ions and N_2 were facilitated by trace nitrogen in the buffer gas. A low amplitude RF pulse on resonance with the secular frequency of the untagged parent ion was applied to remove these ions from the trap. After sweeping, infrared pulses were loosely focused into the trap through a KBr window using a spherical mirror. All ions remaining after the laser interactions were extracted into a reflectron time-of-flight (TOF) mass spectrometer (Jordan TOF). Ion signal was detected with a dual-channel microchannel plate (MCP) detector. The photodissociation yield was calculated as the ratio between parent ion intensity and the sum of intensity of all tagged ions. For both $Re(CO)_3(CH_3CN)_3^+$ and protonated caffeine, up to 4 tags (i.e., $Re(CO)_3(CH_3CN)_3^+ \cdot kN_2$, k = 1 - 4) were observed and included in photodissociation yield calculations. As in our previous report,[2] $Re(CO)_3(CH_3CN)_3^+$ was the dominant ion among a series of ions with formula $Re(CO)_n(CH_3CN)_{6-n}^+$ (n = 1-5).

II. Pulse train generation

The output of a Ti:Sapphire oscillator/regenerative amplifier system (Coherent Astrella, 800 nm, 1 kHz, 35 fs, 3.6 mJ/pulse) was used to pump a commercial OPA system (Light Conversion, TOPAS Prime) to generate tunable near-IR signal (1.2−1.7 μm) and idler (1.7−2.4 μm) pulses. The signal and idler beams were then mixed in a home-built difference frequency generation (DFG) set up with a type I $AgGaS_2$ crystal to generate tunable mid-infrared pulses between 3 to 7 μm (>25 μJ/pulse, >200 cm^{-1} bandwidth, 80-100 fs pulse durations). To collect 2D spectra for $Re(CO)_3(CH_3CN)_3^+$ ions, the laser center frequency was set to around 2050 cm^{-1} with pulse energies ~35 μJ/pulse. The DFG output was sent to a mid-infrared acousto-optic pulse shaper (PhaseTech, Quickshape+) and shaped into a train of four pulses with desired delay, phase, and rotating frame frequency.[2,3] Dispersion and Bragg corrections were applied to compress the pulse in time and optimize output power.[4] The amplitude of the acoustic wave was reduced to avoid signal saturation, and approximately 3 μJ/pulse train of energy entered the ion trap. For protonated caffeine, the DFG output was tuned to 1750 cm^{-1} with pulse energies ~27 μJ/pulse. The maximum output from the shaper at this frequency range was ~ 9 μJ/pulse. The full power was used to interact with protonated caffeine due to its smaller IR response compared to the metal carbonyl species. The amplitude of all four pulses in the pulse train were equivalent, thus the individual pulses in the four-pulse train had energies ~0.75 μJ for $Re(CO)_3(CH_3CN)_3^+$ and ~ 2 μJ for protonated caffeine. The photodissociation yield with a basic mask (when all four pulses are overlapping at time zero) for both species was about 55%.

III. Phase-cycling scheme in 2D experiments

The tag-loss action response due to interaction with the set of four ultrafast pulses was recorded by the photodissociation yield at the MCP detector. Many background pathways coexist with the desired nonlinear signals. For instance, each pair of pulses contribute a linear signal and every set of three pulses generate a transient absorption background. In order to select desired 2D signals, we used phase cycling to remove unwanted signals. Each nonlinear pathway carries a phase dependence that is the linear combination of phases of each pulses in the pulse train. For rephasing and nonrephasing pathways, the phase dependencies are $-\varphi_1+\varphi_2+\varphi_3-\varphi_4$ and $+\varphi_1-\varphi_2+\varphi_3-\varphi_4$, respectively[5] ($\varphi_i$ is the phase of the ith pulse, the first pulse in time is φ_1). The background linear pathway induced by the first and third pulses, for example, has a phase dependency of $+\varphi_1-\varphi_3$. Phase cycling separates pathways with different phase dependencies by adding/subtracting pulse sequences with the appropriate sets of phases and coefficients. Tan et al.[6] proposed a general method for designing phase-cycling schemes, which we described in detail in our previous study.[2] By summing phase-modulated signals with the proper coefficients, rephasing and nonrephasing signals can be obtained from the same data set. Purely absorptive spectra can be obtained by summing the rephasing and nonrephasing spectra in either the time or frequency domains.[7] A 27-step phase-cycling scheme was employed in the current 2D experiments by iterating the phases of the first three pulses through $(0, \frac{2\pi}{3}, \frac{4\pi}{3})$ and fixing the phase of the last pulse at 0. This is equivalent to the most common 27-step phase-cycling scheme for action-detected four-pulse experiment in

electronic spectroscopy.[8,9] The following table shows all sets of phases and coefficients used in this study.

Step	1st	2nd	3rd	4th	Real			Imaginary		
					Abs	R	NR	Abs	R	NR
1	0	0	0	0	0	0	0	2	1	1
2	0	0	$2\pi/3$	0	-1.732	-0.866	-0.866	-1	-0.5	-0.5
3	0	0	$4\pi/3$	0	1.732	0.866	0.866	-1	-0.5	-0.5
4	0	$2\pi/3$	0	0	0	-0.866	0.866	-1	-0.5	-0.5
5	0	$2\pi/3$	$2\pi/3$	0	0.866	0.866	0	0.5	-0.5	1
6	0	$2\pi/3$	$4\pi/3$	0	-0.866	0	-0.866	0.5	1	-0.5
7	0	$4\pi/3$	0	0	0	0.866	-0.866	-1	-0.5	-0.5
8	0	$4\pi/3$	$2\pi/3$	0	0.866	0	0.866	0.5	1	-0.5
9	0	$4\pi/3$	$4\pi/3$	0	-0.866	-0.866	0	0.5	-0.5	1
10	$2\pi/3$	0	0	0	0	0.866	-0.866	-1	-0.5	-0.5
11	$2\pi/3$	0	$2\pi/3$	0	0.866	0	0.866	0.5	1	-0.5
12	$2\pi/3$	0	$4\pi/3$	0	-0.866	-0.866	0	0.5	-0.5	1
13	$2\pi/3$	$2\pi/3$	0	0	0	0	0	2	1	1
14	$2\pi/3$	$2\pi/3$	$2\pi/3$	0	-1.732	-0.866	-0.866	-1	-0.5	-0.5
15	$2\pi/3$	$2\pi/3$	$4\pi/3$	0	1.732	0.866	0.866	-1	-0.5	-0.5
16	$2\pi/3$	$4\pi/3$	0	0	0	-0.866	0.866	-1	-0.5	-0.5
17	$2\pi/3$	$4\pi/3$	$2\pi/3$	0	0.866	0.866	0	0.5	-0.5	1
18	$2\pi/3$	$4\pi/3$	$4\pi/3$	0	-0.866	0	-0.866	0.5	1	-0.5
19	$4\pi/3$	0	0	0	0	-0.866	0.866	-1	-0.5	-0.5
20	$4\pi/3$	0	$2\pi/3$	0	0.866	0.866	0	0.5	-0.5	1
21	$4\pi/3$	0	$4\pi/3$	0	-0.866	0	-0.866	0.5	1	-0.5
22	$4\pi/3$	$2\pi/3$	0	0	0	0.866	-0.866	-1	-0.5	-0.5
23	$4\pi/3$	$2\pi/3$	$2\pi/3$	0	0.866	0	0.866	0.5	1	-0.5
24	$4\pi/3$	$2\pi/3$	$4\pi/3$	0	-0.866	-0.866	0	0.5	-0.5	1
25	$4\pi/3$	$4\pi/3$	0	0	0	0	0	2	1	1
26	$4\pi/3$	$4\pi/3$	$2\pi/3$	0	-1.732	-0.866	-0.866	-1	-0.5	-0.5
27	$4\pi/3$	$4\pi/3$	$4\pi/3$	0	1.732	0.866	0.866	-1	-0.5	-0.5

The first column is the phase cycling step. The middle four columns are the phases for each individual pulse during each phase-cycling step. The last six columns are the real and imaginary part of coefficients calculated for absorptive (Abs), rephasing (R) and nonrephasing (NR) pathways. The time-domain signal is processed as the sum of the coefficient-weighted photodissociation yield of each phase-cycling step:

$$\text{Signal}_{\text{real}} = \sum_{\text{Step Number}} \text{real\_coefficient} \times \text{Signal}_{\text{Step Number}}$$

$$\text{Signal}_{\text{imag}} = \sum_{\text{Step Number}} \text{imag\_coefficient} \times \text{Signal}_{\text{Step Number}}$$

IV. Data acquisition

The mass spectrometer was triggered at 10 Hz by a function generator (DS345, Stanford Research Systems). Ions were stored in the first hexapole guide for 95 ms by placing a repelling voltage on its exit aperture. The pulse valve fired 3 ms after the ions exit the first guide to match the ions' arrival time to the trap. The gas burst had a duration of ~35 ms. An RF sweeping pulse on resonance with the secular frequency of the untagged parent ion was applied between 30 to 40 ms to remove untagged parents. Ions interacted with the laser pulses between 40 to 95 ms, at which time the exit electrode of the ion trap was triggered to extract ions into the TOF region.

The pulse shaper was triggered by the Ti:Sapphire laser system at 1000 Hz repetition rate. A series of mask files were uploaded to the memory of an arbitrary waveform generator (AWG, PXDAC4800, Signatec) before the experiment started. Those masks were programmed by LabVIEW (National Instruments) and controlled the waveform of the acoustic wave, which shaped the input laser pulse into four pulses in time. When receiving a start data collection signal, one of the masks was set active and sent into an RF amplifier, which modulated the digital signal into an acoustic wave that propagated through the germanium AOM crystal. The crystal served as a programmable diffraction grating, allowing for pulse shaping in the frequency domain. For each mass spectrometer cycle (10 Hz), 100 identical pulse trains were directed into the trap to accumulate photoproduct intensity. 16 mass spectrometer cycles were averaged for photodissociation yield of one pulse train (i.e., the same mask was used to shape the ultrafast laser pulse 1600 times, averaged over 16 mass spectrometer cycles). The data collection program would send a switching signal to the AWG after finishing data collection of the previous mask. AWG would stop current mask and would start the next mask immediately.

To collect a 2D spectra at a fixed waiting time (T_w), both pump pulse delays (τ_1) and probe pulse delays (τ_3) needed to be scanned to frequency resolve the two axes. A normal scan for single 2D spectra with 4 fs step from 0 to 5000 fs and 27-step phase cycling at each grid point (τ_1, τ_3) for both axes is not practically possible. Therefore, we made several modifications for data collection scheme. First, each time axis was reduced to 44 points. This reduced total collection time at the cost of lower but acceptable frequency resolution (from 6.67 cm^{-1} to about 13 cm^{-1} (Re cation) or 22 cm^{-1} (protonated caffeine)). Second, a rotating frame of 1400 cm^{-1} (protonated caffeine) or 1900 cm^{-1} (Re cation) was used to phase shift the first (first pump) and last (second probe) pulse in pulse train. Briefly, a rotating frame applies an additional constant frequency phase shift to the pulses, which rotate and downshift the collected signal. The signal will therefore oscillate at a lower frequency and a larger step size can be used while avoiding undersampling. Step sizes of 35 fs (protonated caffeine) and 60 fs (Re cation) were used. Those strategies enabled collecting a single 2D spectrum within 24 hours of acquisition time.

18

V. Data processing

At each grid point (τ_1, τ_3) at a given waiting time T_w, the photodissociation yield of 27 phase-cycling steps were weighted by the appropriate coefficient for rephasing, nonrephasing or absorptive pathways and summed up. After obtaining full 2D time domain data, it was Fourier transformed along τ_3 axis first and then τ_1 axis to be converted into frequency domain. Zero padding with five times the length of signal (220 zeroes) was employed along both τ_1 and τ_3 axes to interpolate the data. A Hanning window was used apodize the time-domain data. Since all four pulses were generated with the same pulse shaper and their phases were controlled, phase correction was not required in data processing.

VI. Supplementary References

(1)   Chen, L.; Dean, J. L. S.; Fournier, J. A. Time-Domain Vibrational Action Spectroscopy of Cryogenically Cooled, Messenger-Tagged Ions Using Ultrafast IR Pulses. *J. Phys. Chem. A* **2021**, *125* (47), 10235–10244.

(2)   Chen, L.; Ma, Z.; Fournier, J. A. Ultrafast Transient Vibrational Action Spectroscopy of Cryogenically Cooled Ions. *J. Chem. Phys.* **2023**, *159* (4), 041101.

(3)   Shim, S.-H.; Strasfeld, D. B.; Ling, Y. L.; Zanni, M. T. Automated 2D IR Spectroscopy Using a Mid-IR Pulse Shaper and Application of This Technology to the Human Islet Amyloid Polypeptide. *Proc. Natl. Acad. Sci.* **2007**, *104* (36), 14197–14202.

(4)   Jones, A. C.; Kunz, M. B.; Tigges-Green, I.; Zanni, M. T. Dual Spectral Phase and Diffraction Angle Compensation of a Broadband AOM 4-f Pulse-Shaper for Ultrafast Spectroscopy. *Opt. Express* **2019**, *27* (26), 37236–37247.

(5)   Perdomo-Ortiz, A.; Widom, J. R.; Lott, G. A.; Aspuru-Guzik, A.; Marcus, A. H. Conformation and Electronic Population Transfer in Membrane-Supported Self-Assembled Porphyrin Dimers by 2D Fluorescence Spectroscopy. *J. Phys. Chem. B* **2012**, *116* (35), 10757–10770.

(6)   Yan, S.; Tan, H.-S. Phase Cycling Schemes for Two-Dimensional Optical Spectroscopy with a Pump–Probe Beam Geometry. *Chem. Phys.* **2009**, *360* (1), 110–115.

(7)   Hamm, P.; Zanni, M. *Concepts and Methods of 2D Infrared Spectroscopy*; Cambridge University Press, 2011.

(8)   Draeger, S.; Roeding, S.; Brixner, T. Rapid-Scan Coherent 2D Fluorescence Spectroscopy. *Opt. Express* **2017**, *25* (4), 3259–3267.

(9)   De, A. K.; Monahan, D.; Dawlaty, J. M.; Fleming, G. R. Two-Dimensional Fluorescence-Detected Coherent Spectroscopy with Absolute Phasing by Confocal Imaging of a Dynamic Grating and 27-Step Phase-Cycling. *J. Chem. Phys.* **2014**, *140* (19), 194201.

VII. Imaginary components of the absorptive, rephasing, and nonrephasing signal
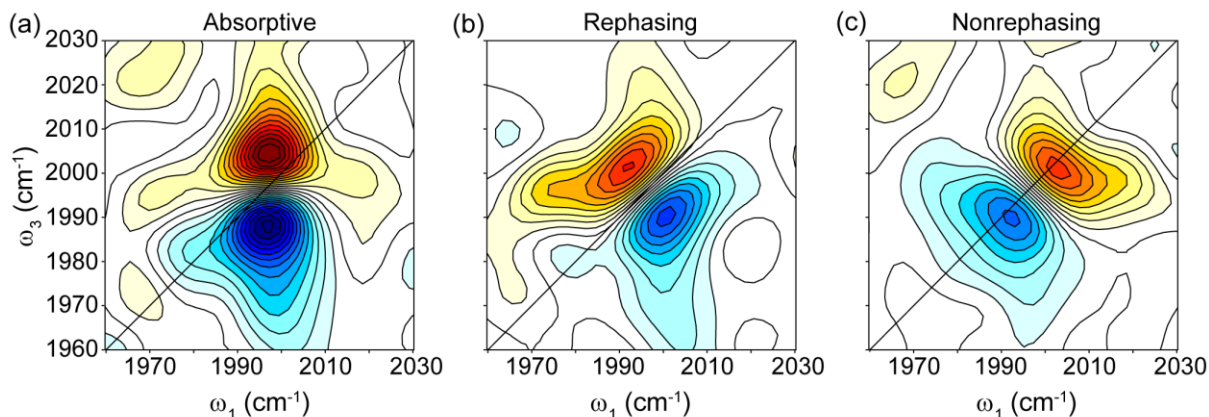
Imaginary components of the (a) absorptive, (b) rephasing, and (c) nonrephasing signals of the asymmetric carbonyl stretch in *fac*-Re(CO)$_3$(CH$_3$CN)$_3^+$ at 417 fs waiting time. Like the real components shown in main text Fig. 3, the imaginary rephasing and nonrephasing signals illustrate the expected phase twists due to contributions from absorptive and dispersive lineshape components.

VIII. 4th-order Feynman diagrams

The following are the rephasing double-sided Feynman diagrams for two uncoupled oscillators A and S that give rise to ground-state bleach (GSB), stimulated emission (SE), and excited-state absorption (ESA) signals along the diagonal. The GSB and SE signals are proportional to $-|\langle 1|\mu|0\rangle|^4 e^{-i\omega_{10}(\tau_3-\tau_1)}$. The ESA1 pathway signal is $-|\langle 2|\mu|1\rangle|^2|\langle 1|\mu|0\rangle|^2 e^{i\omega_{10}\tau_1} e^{-i\omega_{21}\tau_3}$. The ESA2 pathway signal is proportional is $+|\langle 2|\mu|1\rangle|^2|\langle 1|\mu|0\rangle|^2 e^{i\omega_{10}\tau_1} e^{-i\omega_{21}\tau_3}$.
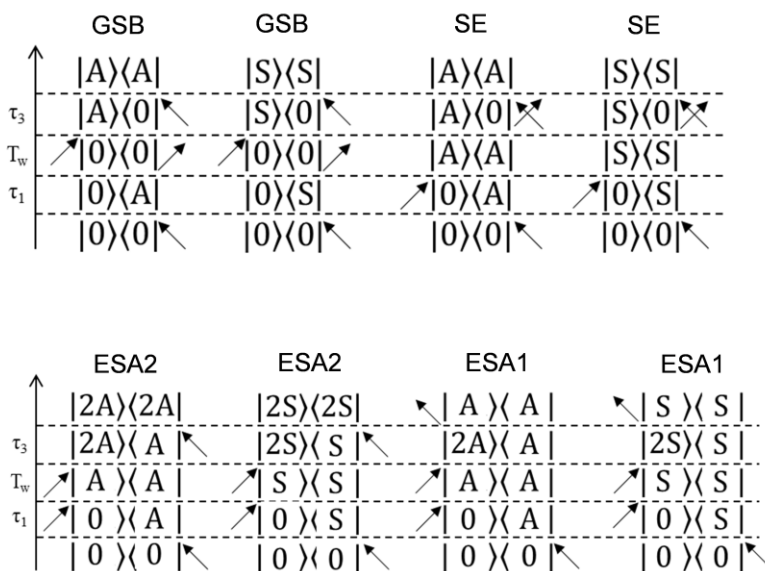
The following are the nonrephasing double-sided Feynman diagrams for two uncoupled oscillators A and S that give rise to ground-state bleach (GSB), stimulated emission (SE), and excited-state absorption (ESA) signals along the diagonal. The GSB and SE signals are proportional to $-|\langle 1|\mu|0\rangle|^4 e^{-i\omega_{10}(\tau_3+\tau_1)}$. The ESA1 pathway signal is $-|\langle 2|\mu|1\rangle|^2|\langle 1|\mu|0\rangle|^2 e^{-i\omega_{10}\tau_1}e^{-i\omega_{21}\tau_3}$. The ESA2 pathway signal is $+|\langle 2|\mu|1\rangle|^2|\langle 1|\mu|0\rangle|^2 e^{-i\omega_{10}\tau_1}e^{-i\omega_{21}\tau_3}$.

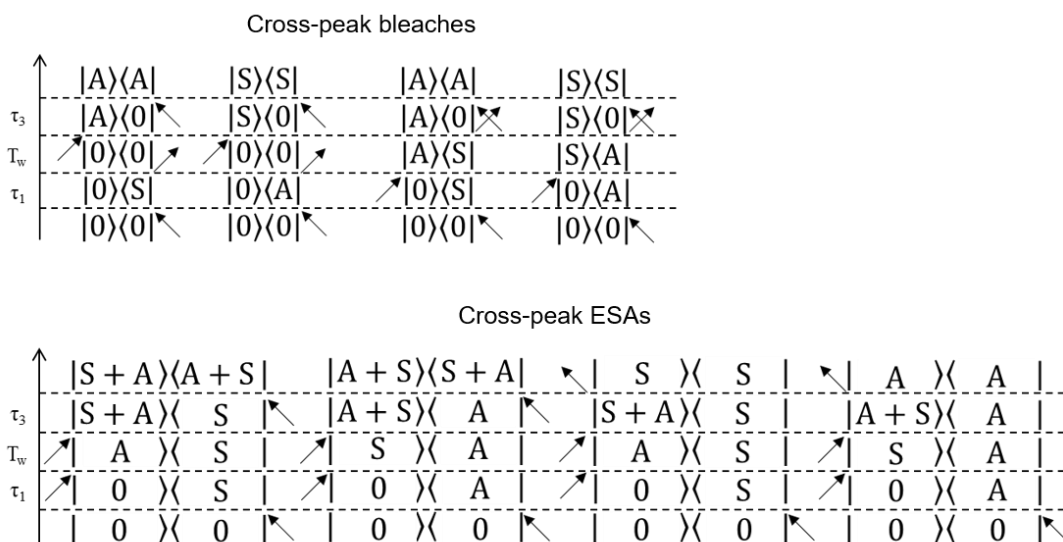|	GSB	GSB	SE	SE
	$|A\rangle\langle A|$	$|S\rangle\langle S|$	$|A\rangle\langle A|$	$|S\rangle\langle S|$
τ_3	$|A\rangle\langle 0|$	$|S\rangle\langle 0|$	$|A\rangle\langle 0|$	$|S\rangle\langle 0|$
T_w	$|0\rangle\langle 0|$	$|0\rangle\langle 0|$	$|A\rangle\langle A|$	$|S\rangle\langle S|$
τ_1	$|A\rangle\langle 0|$	$|S\rangle\langle 0|$	$|A\rangle\langle 0|$	$|S\rangle\langle 0|$
	$|0\rangle\langle 0|$	$|0\rangle\langle 0|$	$|0\rangle\langle 0|$	$|0\rangle\langle 0|$

	ESA2	ESA2	ESA1	ESA1
	$|2A\rangle\langle 2A|$	$|2S\rangle\langle 2S|$	$|A\rangle\langle A|$	$|S\rangle\langle S|$
τ_3	$|2A\rangle\langle A|$	$|2S\rangle\langle S|$	$|2A\rangle\langle A|$	$|2S\rangle\langle S|$
T_w	$|A\rangle\langle A|$	$|S\rangle\langle S|$	$|A\rangle\langle A|$	$|S\rangle\langle S|$
τ_1	$|A\rangle\langle 0|$	$|S\rangle\langle 0|$	$|A\rangle\langle 0|$	$|S\rangle\langle 0|$
	$|0\rangle\langle 0|$	$|0\rangle\langle 0|$	$|0\rangle\langle 0|$	$|0\rangle\langle 0|$
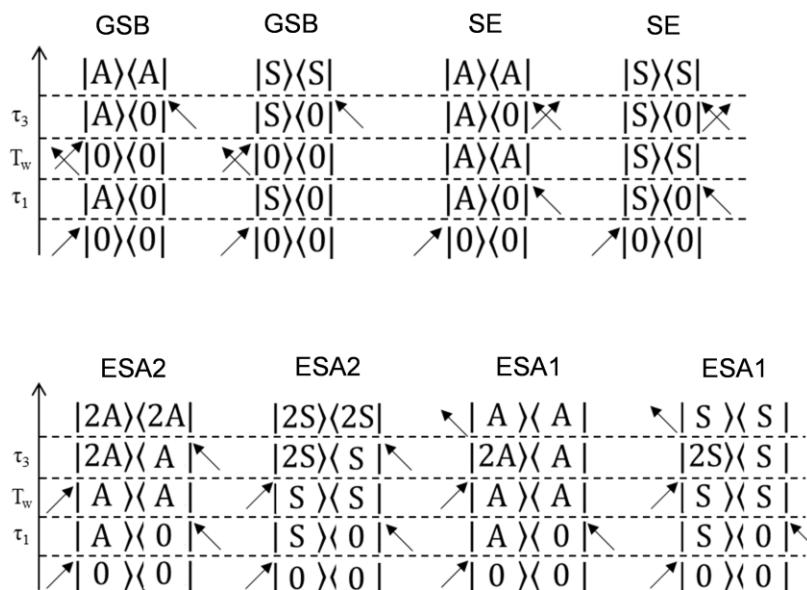
The following are the rephasing double-sided Feynman diagrams for two coupled oscillators A and S that give rise to bleach and excited-state cross-peak signals. Pathways in the $|A\rangle\langle S|$ or $|S\rangle\langle A|$ state during T_w are called interstate coherences and evolve as $e^{-i\omega_{AS}T_w}$. These pathways result in the oscillatory nature of the TA and 2D signals in $Re(CO)_3(CH_3CN)_3{}^+$.

Cross-peak bleaches

	$|A\rangle\langle A|$	$|S\rangle\langle S|$	$|A\rangle\langle A|$	$|S\rangle\langle S|$
τ_3	$|A\rangle\langle 0|$	$|S\rangle\langle 0|$	$|A\rangle\langle 0|$	$|S\rangle\langle 0|$
T_w	$|0\rangle\langle 0|$	$|0\rangle\langle 0|$	$|A\rangle\langle S|$	$|S\rangle\langle A|$
τ_1	$|0\rangle\langle S|$	$|0\rangle\langle A|$	$|0\rangle\langle S|$	$|0\rangle\langle A|$
	$|0\rangle\langle 0|$	$|0\rangle\langle 0|$	$|0\rangle\langle 0|$	$|0\rangle\langle 0|$

Cross-peak ESAs

	$|S+A\rangle\langle A+S|$	$|A+S\rangle\langle S+A|$	$|S\rangle\langle S|$	$|A\rangle\langle A|$
τ_3	$|S+A\rangle\langle S|$	$|A+S\rangle\langle A|$	$|S+A\rangle\langle S|$	$|A+S\rangle\langle A|$
T_w	$|A\rangle\langle S|$	$|S\rangle\langle A|$	$|A\rangle\langle S|$	$|S\rangle\langle A|$
τ_1	$|0\rangle\langle S|$	$|0\rangle\langle A|$	$|0\rangle\langle S|$	$|0\rangle\langle A|$
	$|0\rangle\langle 0|$	$|0\rangle\langle 0|$	$|0\rangle\langle 0|$	$|0\rangle\langle 0|$

The following are the nonrephasing double-sided Feynman diagrams for two coupled oscillators A and S that give rise to bleach and excited-state cross-peak signals.

Cross-peak bleaches

Cross-peak ESAs